Journal of Solid State Chemistry 183 (2010) 883–889

Contents lists available at ScienceDirect

Journal of Solid State Chemistry

journal homepage: www.elsevier.com/locate/jssc

Morphological and structural evolution of α-MnO_2 nanorods synthesized via an aqueous route through MnO_4^-/Mn^{2+} reaction

Xiaobo Fu [a,b], Jiyun Feng [a,*], Huan Wang [a,b], Ka Ming Ng [a,b]

[a] Nano and Advanced Materials Institute Limited, Clear Water Bay, Kowloon, Hong Kong
[b] Department of Chemical and Biomolecular Engineering, The Hong Kong University of Science and Technology, Clear Water Bay, Kowloon, Hong Kong

ARTICLE INFO

Article history:
Received 28 October 2009
Received in revised form
1 February 2010
Accepted 5 February 2010
Available online 10 February 2010

Keywords:
Manganese dioxide
Nanorods
Crystallization-dissolution
Catalytic oxidation

ABSTRACT

An aqueous route through MnO_4^-/Mn^{2+} reaction under mild conditions was used to synthesize α-MnO_2 nanorods. The morphological and structural evolution of α-MnO_2 nanorods during their growth were tracked by Powder X-ray diffraction (XRD), scanning electron microscopy (SEM), transmission electron microscopy (TEM) and BET analysis. The crystallization of α-MnO_2 nanorods was found to proceed through three steps: (1) Amorphous or poorly ordered nuclei formed first. (2) Then hollow nanoshperes consisting of γ-MnO_2 nanorods formed via the Ostwald ripening process. (3) The hollow nanospheres broke down and the γ-MnO_2 nanorods finally transformed into the α-MnO_2 nanorods with increasing temperature or reaction time. The phase transformation from γ-MnO_2 to α-MnO_2 nanorods was accomplished by a short-range rearrangement of MnO_6 octahedra. In addition, the performance of the MnO_2 materials as a catalyst was evaluated in the aerobic oxidation of benzyl alcohol, showing that their catalytic activities were mainly dependent on their BET surface areas.

1. Introduction

Nanometer-sized materials have exhibited extraordinarily different electronic, magnetic, catalytic, optical, and other properties from those of their corresponding bulk materials [1]. Rational synthesis of such materials with controllable crystal structures, morphologies and sizes is very important because the properties of the materials can be tuned with flexibility [2,3]. Among various routes to obtain such materials, aqueous route is a promising one since it provides versatile control over the nucleation/growth process through many operational parameters [4,5]. Moreover, it is very attractive owing to its low environmental impact, simple operation and low cost.

Recently, manganese dioxide (MnO_2) has attracted growing interest due to its structure flexibility and potential applications in many areas [6–8], such as energy storage [9] and redox catalysis [10]. In fact, most studies on the synthesis of the MnO_2 nanomaterials are focused on structural and morphological control and involve aqueous precipitation [11–13]. Therefore, three dimensional (hierarchical ε-MnO_2) [14], two dimensional (birnessite-type δ-MnO_2 layered manganese oxides) [15,16] and one dimensional (tunnel-based frameworks: cryptomelane-type α-MnO_2, γ-MnO_2, pyrolusite β-MnO_2) nanostructures [17–20] have been developed. However, because of the polymorphs of the MnO_2, the synthesis control for the preparation of single phase MnO_2 is still a big challenge even though some pure crystalline phases were prepared by varying the synthesis parameters. Thus, understanding the nucleation and crystallization mechanisms for the synthesizing single phase MnO_2 under aqueous conditions is expected to have both academic and industrial significance for the improved control of crystal structures, morphologies and sizes of MnO_2 nanostructures.

The reaction between the MnO_4^- and Mn^{2+} in aqueous solution has been proven to be a versatile route to the synthesis of MnO_2 nanostructures because it provides many experimental parameters to modify the reaction pathway [5,21–23]. In this work, we report the synthesis of the α-MnO_2 nanorods via an aqueous route through MnO_4^-/Mn^{2+} reaction at low temperature ($\leq 95\,^{\circ}C$) in the presence of the excess amount of Mn^{2+}. The morphological and structural evolution during growth of the α-MnO_2 nanorods were tracked by XRD, SEM, TEM and BET analysis. The phase transformation mechanism for γ-MnO_2 to α-MnO_2 nanorods was discussed. The catalytic activity and selectivity of the obtained MnO_2 products were also evaluated in the aerobic oxidation of benzyl alcohol.

2. Experimental details

2.1. Synthesis of α-MnO_2 nanorods

Analytical grade $MnSO_4 \cdot H_2O$ (8.50 g) and $KMnO_4$ (3.43 g) ($MnSO_4$ to $KMnO_4$ mole ratio=2.3) powders were ground together

* Corresponding author. Fax: +852 23588113.
E-mail address: kejyfeng@ust.hk (J. Feng).

0022-4596/$ - see front matter © 2010 Elsevier Inc. All rights reserved.
doi:10.1016/j.jssc.2010.02.002

for 1 h in an automatic mortar at room temperature. Then, two sets of experiments were performed as follows:

In the first set of experiments, the mixed powder was transferred to 200 mL distilled water in a beaker under continuous electromagnetic stirring at three different temperatures (room temperature, 60 °C or 95 °C). Then, another 100 mL of 1 M H_2SO_4 solution was added to the beaker. After reaction for 17 h, the precipitates were filtered and rinsed with distilled water and ethanol to remove any chemical species possibly remaining in the final products. The resultant products were then dried in an oven at 70 °C overnight.

In the second set of experiments, the mixed powder was transferred to 200 mL distilled water in a beaker under continuous electromagnetic stirring at room temperature. Then, another 100 mL of 1 M H_2SO_4 solution was added to the beaker. The reaction at room temperature was kept for 0.5 h. After that, the reaction system was immediately transferred to 95 °C water bath with a condensator for different reaction times. After reaction, the treatment of the products was the same as described above.

2.2. Characterization

The X-ray powder diffraction (XRD) analysis of the products was performed on a PAnalytical X'pert Pro X-ray Diffractometer equipped with Cu-Kα radiation (λ=1.54178 Å), operating at 40 kV and 40 mA. The morphologies of the products were observed by a field emission scanning electron microscope (FESEM, JEOL JSM-6700F) with an accelerating voltage of 5 kV. Prior to the SEM observation, the samples were sputtered with a thin layer of gold to reduce the charging effect. Electron micrographs of the products were taken using a TEM (TEM, JEOL-2100F) with an accelerating voltage of 200 kV, equipped with a Bruker energy dispersive X-ray spectroscopy (EDXS). The TEM samples were prepared by dropping an acetone dispersion of the different products onto a copper grid coated with a holey amorphous carbon, followed by drying in a vacuum desiccator. The BET-specific surface area was determined by N_2 adsorption at 77 K using a Micromeritics ASAP 2000 system after the sample was degassed in vacuum at 130 °C overnight.

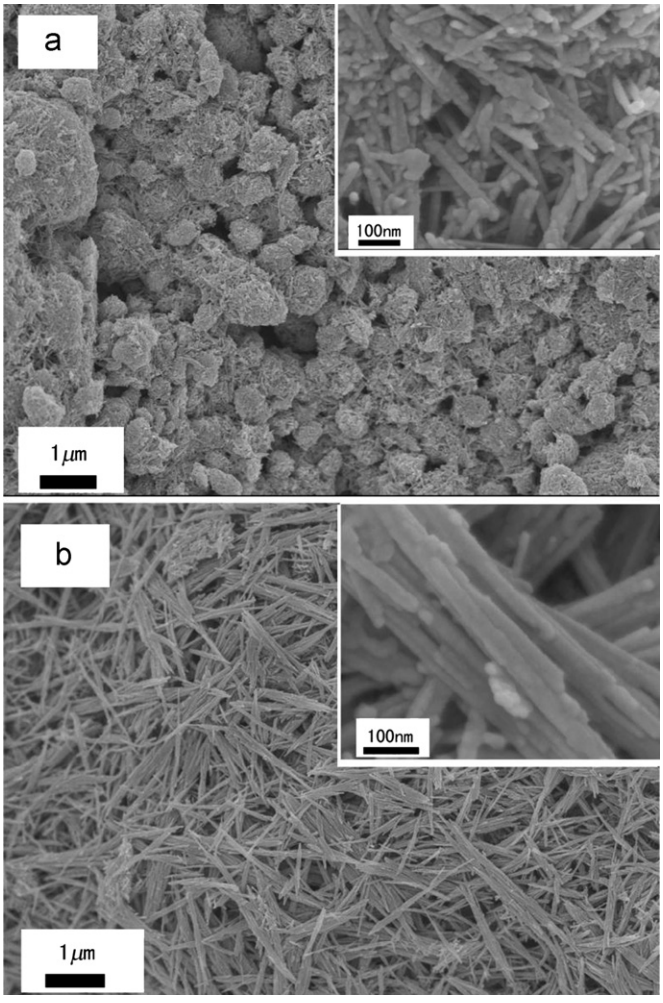

Fig. 1. SEM images of the MnO_2 materials prepared at (a) 60 °C and (b) 95 °C with a constant reaction time of 17 h.

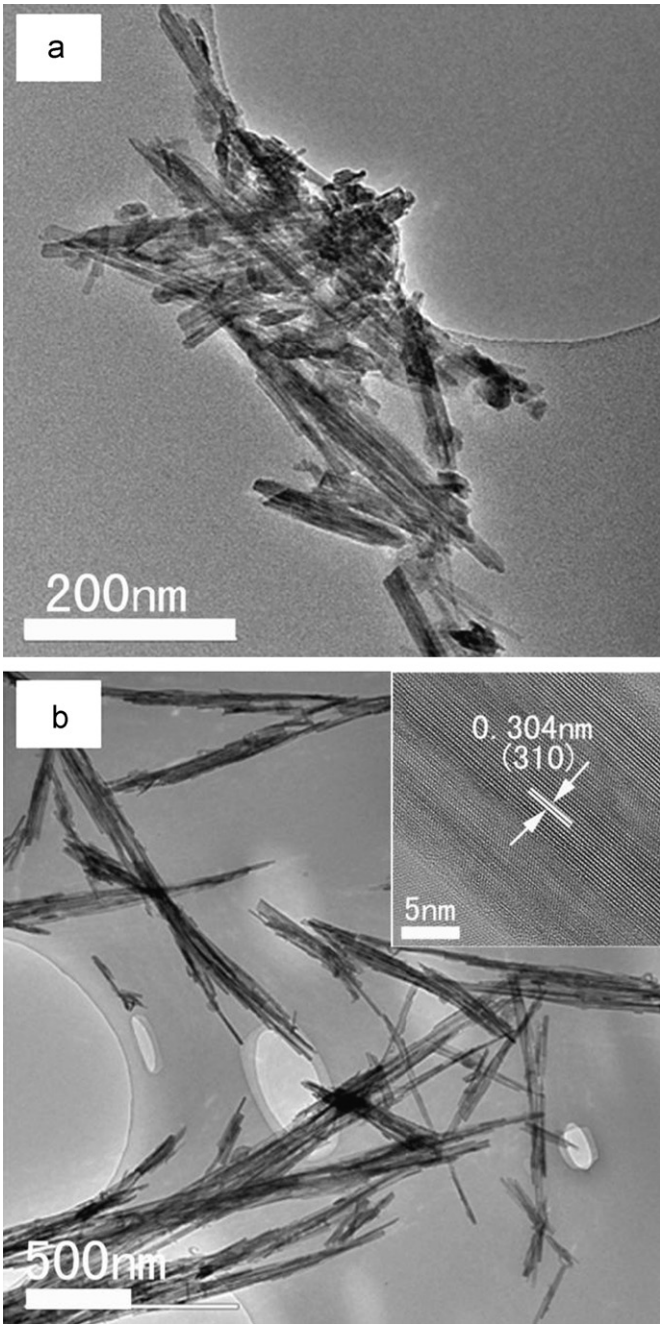

Fig. 2. TEM images of the MnO_2 materials prepared at (a) 60 °C and (b) 95 °C with a constant reaction time of 17 h (the inset is a HRTEM image of single α-MnO_2 nanorod).

2.3. Catalytic activity test

For a typical procedure of the alcohol oxidation, toluene (10 mL) and benzyl alcohol (1 mmol) were first added to a 25 mL round-bottomed flask containing 0.05 g catalyst. The mixture was then stirred under reflux at 110 °C with air bubbling. The air was controlled by a mass flow controller with a flow rate of 10 mL/min. After reaction for 2 h, the reaction mixture was cooled down to room temperature. The filtrate was analyzed using a gas chromatography/mass spectrometry (GC/MS).

3. Results and discussion

3.1. Morphological and structural evolution of α-MnO_2 nanorods

Fig. 1 shows the SEM images of the MnO_2 materials prepared by an aqueous reaction between MnO_4^- and Mn^{2+} at different temperatures with a constant reaction time of 17 h. The morphology of the MnO_2 materials synthesized at room temperature has been reported in our previous work [24,25], which showed aggregated hollow nanospheres consisting of nanorods interwined together. With the reaction temperature was increased to 60 °C, the product obtained was still made up of hollow nanospheres with diameter of about 300–900 nm. These hollow nanospheres tended to break up. As shown in the inset of Fig. 1a, both the length and diameter of the nanorods increased when compared with those of the product obtained at room temperature. When the reaction temperature was further increased to 95 °C, the hollow nanospheres in the product totally disappeared. Instead, only regular nanorods were observed in the product. The diameter and length of the obtained nanorods are about 10–20 nm and 1–3 μm, respectively. Several bundles consisting of a few nanorods were observed. The same results were observed in TEM characterizations, as shown in Fig. 2. With the temperature increasing, the length and diameter of the nanorods increased. Moreover, when the temperature increased to 95 °C, the HRTEM image (inset of the Fig. 2b) of a single nanorod indicated that the nanorod was uniform and crystalline; the lattice spacing of 0.304 nm is consistent with that of α-MnO_2 (310) plane, indicating the formation of the α-MnO_2 structures. These results illustrate that the growth of nanorods was strongly dependent on the reaction temperature, and a higher reaction temperature promoted the fast growth of the nanorods.

Fig. 3 shows the XRD patterns of MnO_2 products synthesized at different reaction temperatures with the reaction time of 17 h. The crystal structure of the MnO_2 product synthesized at room temperature was reported as pure γ-MnO_2 in our previous work [22,23]. When the reaction temperature was increased to 60 °C,

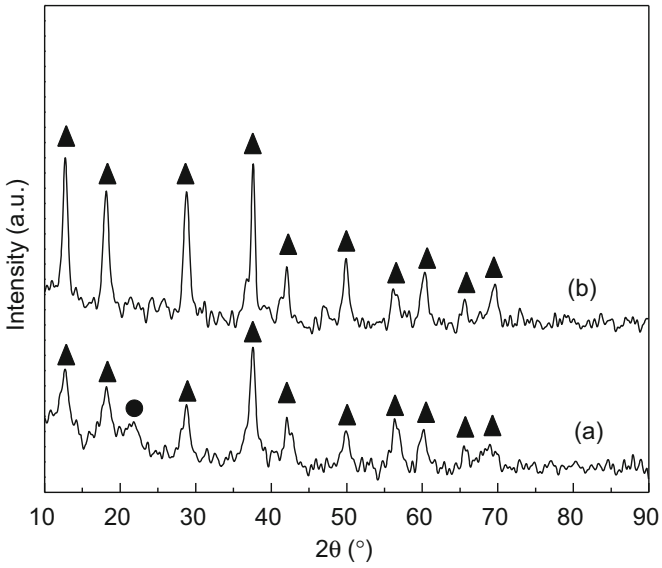

Fig. 3. XRD patterns of MnO_2 materials prepared at (a) 60 °C and (b) 95 °C with a constant reaction time of 17 h. (▲) α-MnO_2; (●) γ-MnO_2.

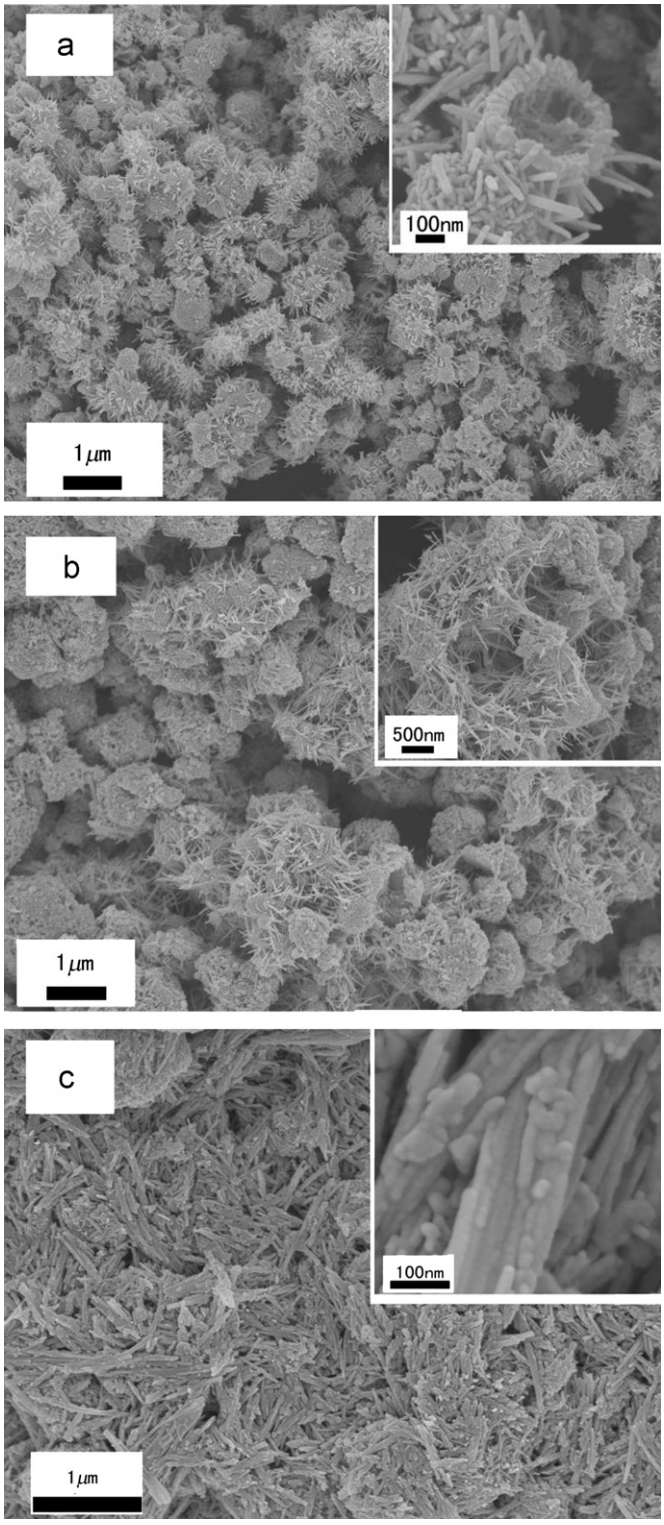

Fig. 4. SEM images of the MnO_2 materials prepared at 95 °C with different reaction time after stirring at room temperature for 0.5 h: (a) 0.5 h; (b) 2 h; (c) 17 h.

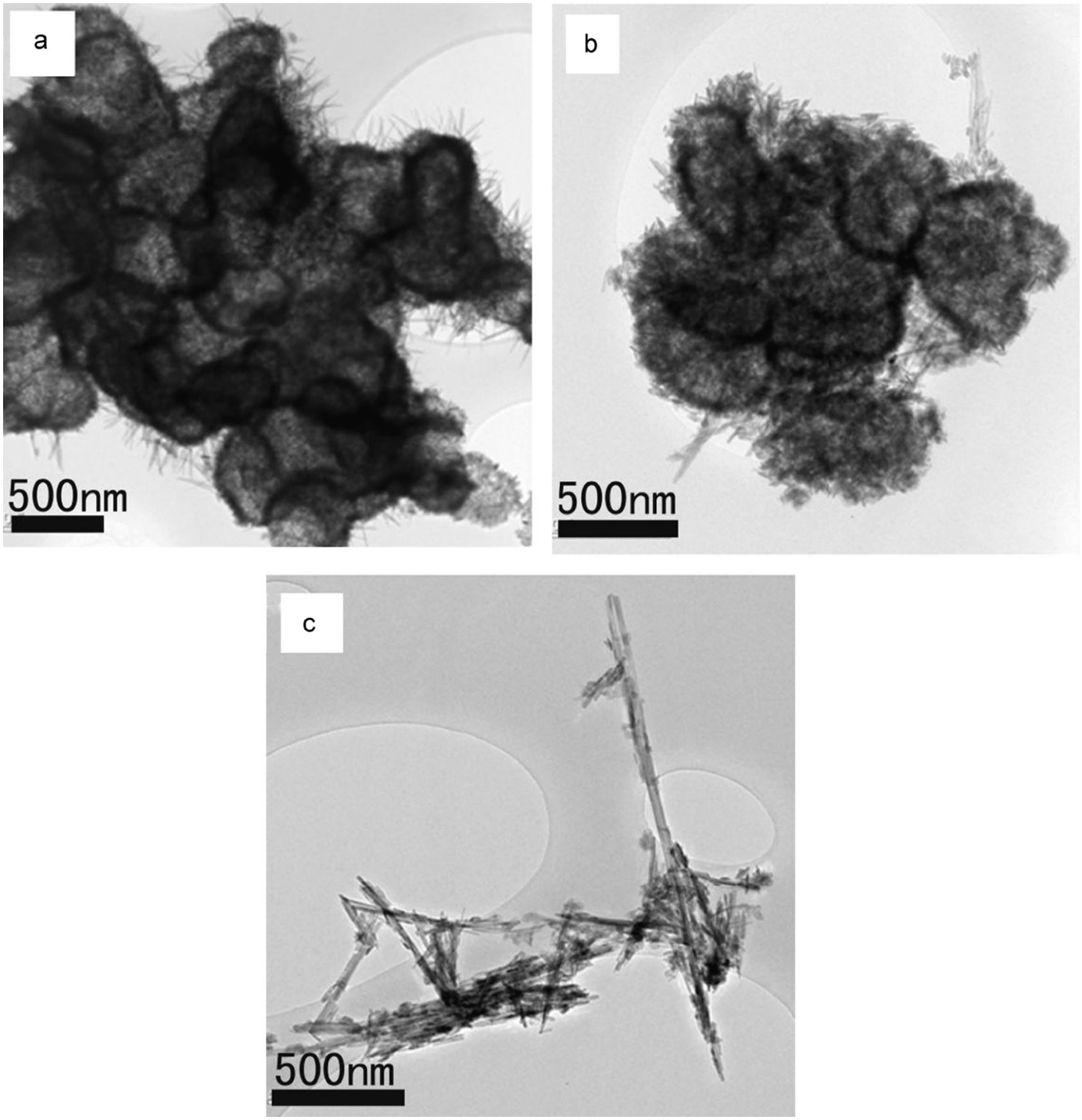

Fig. 5. TEM images of the MnO_2 materials prepared at 95 °C with different reaction time after stirring at room temperature for 0.5 h: (a) 0.5 h; (b) 2 h; (c) 17 h.

both γ-MnO_2 and α-MnO_2 phases were detected in the product, and the diffraction peaks of the α-MnO_2 became more sharp and intense, implying that a gradual transformation from γ-MnO_2 to α-MnO_2 crystallites started. When the reaction temperature was increased to 95 °C, only α-MnO_2 diffraction peaks were detected in the product. This reveals clearly that γ-MnO_2 nanorods transformed completely into α-MnO_2 nanorods, suggesting that a higher reaction temperature is favorable to form α-MnO_2 nanorods.

Figs. 4 and 5 depict the SEM and TEM images of the products prepared by an aqueous reaction between MnO_4^- and Mn^{2+} at a constant reaction temperature of 95 °C with different times after stirring the solution at room temperature for 0.5 h. The early stage of the reaction (0.5 h) yielded hollow nanospheres of MnO_2 materials with diameter of about 300–800 nm consisting of short nanorods. A broken nanosphere in the inset of the Fig. 4a can strongly support that the nanospheres were hollow. At the same time, some nanorods compactly grew out from the surface of the hollow nanospheres. These nanorods grew in length and size as the reaction time increased. When the reaction time was increased to 2 h, seeing Fig. 4b, urchin-like nanospheres started to appear. And the hollow structure was tended to break up which

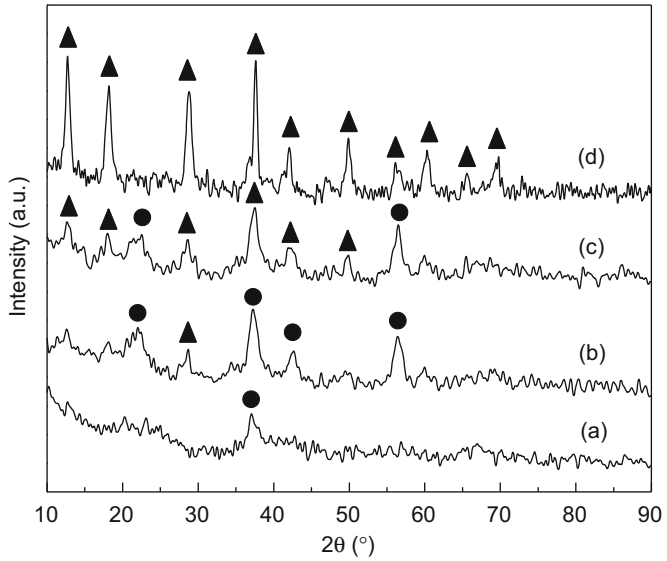

Fig. 6. XRD patterns of MnO_2 materials prepared 95 °C with different reaction time after stirring at room temperature for 0.5 h: (a) 0.5 h; (b) 2 h; (c) 17 h. (▲) α-MnO_2; (●) γ-MnO_2.

might be caused by the increase of the length and size of the nanorods, as can be seen in the inset of the Fig. 4b. After reaction for 17 h, the aqueous reaction yields aggregated nanorods with diameter and length about 10 nm and 1 μm. The results clearly elucidate that an increase in the reaction time leads to collapse of the hollow nanospheres, and formation of nanorods.

The XRD patterns of the products prepared by an aqueous reaction between MnO_4^- and Mn^{2+} at 95 °C with different times after stirring the solution at room temperature for 0.5 h were also measured, and are shown in Fig. 6. After stirring the solution at room temperature for 0.5 h, the XRD pattern in Fig. 6a indicated that the initial precipitates were poorly ordered. When the reaction system was kept at 95 °C for 0.5 h, the characteristic diffraction peaks of γ-MnO_2 appeared, indicating that a higher reaction temperature promoted the growth of MnO_2 nanorods, seeing Fig. 6b. After reaction for 2 h, a mixture of γ-MnO_2 and α-MnO_2 were detected, as shown in Fig. 6c. This indicated that a phase transformation from γ-MnO_2 to α-MnO_2 nanorods started to occur. After reaction for 17 h, all the diffraction peaks of the γ-MnO_2 disappeared and all the diffraction peaks detected can be indexed to α-MnO_2, implying a complete phase transformation from γ-MnO_2 and α-MnO_2, as shown in Fig. 6d. All the results demonstrate that an increase in reaction time promoted the phase transformation.

3.2. Growth and phase transformation of α-MnO_2 nanorods

Based on the morphological and structural evolution studies, it was observed that the formation of α-MnO_2 nanorods from the redox reaction between $KMnO_4$ and $MnSO_4$ involves three processes, i.e. nucleation, growth of γ-MnO_2 crystallites and subsequently phase transformation from γ-MnO_2 to α-MnO_2. Usually, the MnO_2 crystallization proceeds through two steps: a disordered [26] or layered [17,27] manganese oxide precursor is formed, followed by an aging process to form the final product with ordered structure. When the mixture of $KMnO_4$ and $MnSO_4$ after grinding was added into water, the color of the reaction solution changed immediately into light brown, and darken, indicating that the nucleation started. Recently, Suib et al. [27] used *in situ* synchrotron XRD to investigate the morphological and structural evolution of manganese oxide during hydrothermal

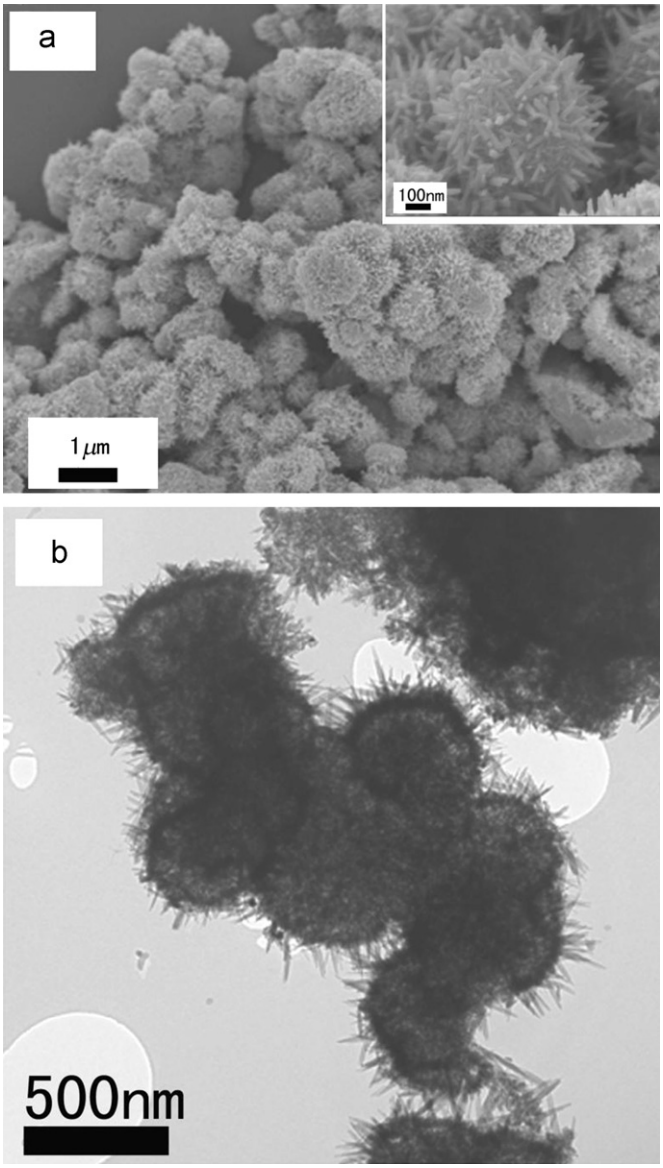

Fig. 7. SEM and TEM images of the MnO_2 product prepared at room temperature for 7 days.

synthesis. They observed that the MnO_6 sheets connected to each other in the early moments of the reaction to form ramsdellite structures in acidic conditions. Gao and coworkers [13] also used *in situ* synchrotron XRD to study the morphological and structural evolution of β-MnO_2 nanorods and they found that the γ-MnO_2 firstly appeared in the acidic environment. This indicated that the early stage of aqueous reaction between MnO_4^- and Mn^{2+} mainly yields the γ-MnO_2. Considering the reaction environment in our process, our results agreed with their findings. This also can be explained by the stability of the polymorphs of the MnO_2. γ-MnO_2 is less stable than the α-MnO_2 and β-MnO_2. Based on the observations above, we found that the growth of the α-MnO_2 crystallites could be promoted by either increasing the reaction temperature (Fig. 1a) or extending the reaction time (Fig. 5a), in which the former process is dominant. This is also supported by the results of reaction at room temperature for 7 days, as shown in Figs. 7 and 8. The morphology and crystal structure of the product are similar to those of the sample prepared at 95 °C with 0.5 h after stirring the solution at room temperature for 0.5 h, demonstrating that the reaction temperature is dominant.

Moreover, the formation mechanism of the γ-MnO_2 hollow structures synthesized at room temperature has been reported as an Ostwald ripening process in our previous work [23]. With the increase in reaction temperature and reaction time, both the length and diameter of the nanorods increase significantly. These observations supported a nucleation-dissolution-crystallization mechanism instead of a rolling mechanism [17]. Although Wang and Li [17] proposed that the formation mechanism of birnessite nanotubes was rolling of ill-defined sheets under hydrothermal conditions, however, such reaction intermediates were not observed in our low-temperature synthesis because the precursor is not enough ordered to form lattice fringes when they were observed by HRTEM. In other words, during the aqueous reaction, the shorter γ-MnO_2 nanorods may re-dissolve into the solution phase due to an acid-etching effect [27], and the longer ones will grow much longer owing to their anisotropic growth behavior [17,27,28]. The formation of the three-dimensional hollow γ-MnO_2 nanostructures seems in harmony with this assumption. However, the final nanorods not only have longer length but also larger diameter. This means that the longitudinal growth is accompanied with lateral growth. Given the higher impact of temperature on longitudinal growth of the nanorods, growth along with the nanorod axis may proceed by another mechanism. The dissolution-crystallization process is temperature dependent because rising temperature increases the solubility of the Mn species, which is in agreement with the length increase of the nanorods with temperature increase. Cassaignon et al. [29] reported that highly acidic media promoted the growth stage by increasing the solubility of Mn species but also limit the growth stage via proton chemisorption stabilizing the surfaces. Thus, stabilization by proton adsorption occurred and it has great impact on the final nanorods morphology by limiting the longitudinal growth. The lateral growth is then believed to be another mechanism.

The phase transformation from γ-MnO_2 to α-MnO_2 can be explained by their structural similarity. It is well known that MnO_2 exists in polymorphs, such as α-, β-, ε- and γ-MnO_2. They are different in the way of the basic unit [MnO_6] octahedra linked [11]. The α-MnO_2 structures are made of edge-shared MnO_6 octahedra forming chains linked together by corners of MnO_6 octahedra. This connectivity thus allows the formation of 1D tunnel structures with *X_X* octahedra cross sections (*X*) (1, 2, 3, or 4). De Wolff [30] proposed that γ-MnO_2 is a ramsdellite (2.3 Å × 4.6 Å tunnel structure) matrix with randomly distributed intergrowth microdomains of pyrolusite (2.3 Å × 2.3 Å tunnel structure), which are constructed of [MnO_6] units with edge or corner sharing. But the ramsdellite is metastable and will transform into α-MnO_2 or β-MnO_2 with increasing temperature. However, due to the mild reaction conditions in this study, β-MnO_2 cannot form. Therefore, the phase transformation from γ-MnO_2 to α-MnO_2 can be considered as the growth of α-MnO_2 in a ramsdellite matrix, which involves a collapse of the 1×2 framework and a subsequent short rearrangement of the MnO_6 octahedra unit.

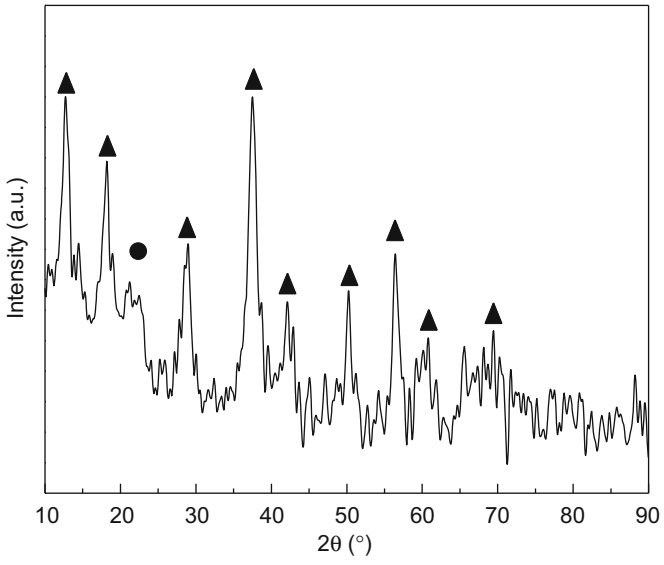

Fig. 8. XRD pattern of the MnO_2 materials prepared at room temperature for 7 days. (▲) α-MnO_2; (●) γ-MnO_2.

3.3. Catalytic activity

MnO_2 materials have been used for allylic and benzylic oxidations, and their catalytic activities depend on the preparations, compositions, crystal structures, and morphologies [31]. Here we used the MnO_2 structures obtained under different conditions as catalysts for aerobic oxidation of benzyl alcohol to benzaldehyde to study the effect of the structure and morphology on their properties, as shown in Table 1. It could be clearly seen that these products are active for catalytic oxidation of benzyl alcohol, giving the benzaldehyde as the main product. The MnO_2 materials obtained at the early stage by room temperature reaction for 0.5 h with highest BET surface areas of 190 m^2/g showed the highest catalytic activity. On the contrary, MnO_2 materials synthesized by direct reaction at 95 °C for 17 h with the lowest BET surface areas of 50 m^2/g showed lowest catalytic activity. In general, it is accepted that the catalytic activity of the MnO_2 materials was dependent on their structures, morphologies and BET surface areas [31]. However, in our synthesis of MnO_2 nanomaterials, with increasing the reaction temperature or prolonging reaction time, the BET surface areas decreased significantly. After fitting the TOF factor with the BET surface

Table 1
Aerobic oxidation of benzyl alcohol using manganese dioxides as catalysts.

Sample	Synthesis condition	BET surface area, m^2/g	Conversion, %	Selectivity, %	TOF[a], h^{-1}
MnO_2	60 °C, 17 h	89	75	> 99	0.33
MnO_2	95 °C, 17 h	50	44	> 99	0.19
MnO_2	25 °C, 0.5 h, 95 °C, 0 h	198	95	> 99	0.42
MnO_2	25 °C, 0.5 h, 95 °C, 0.5 h	130	81	> 99	0.36
MnO_2	25 °C, 0.5 h, 95 °C, 2 h	89	71	> 99	0.31
MnO_2	25 °C, 0.5 h, 95 °C, 17 h	64	59	> 99	0.26
MnO_2	25 °C, 7 days	92	53	> 99	0.23

Reaction conditions: 1 mmol benzyl alcohol, 10 mL toluene, 0.05 g catalyst, *T*=110 °C and pressure=0.1 Mpa; reaction time: 2 h; flow rate of air: 10 mL/min.

[a] Turn over frequency based on substrate per mol MnO_2 per h.

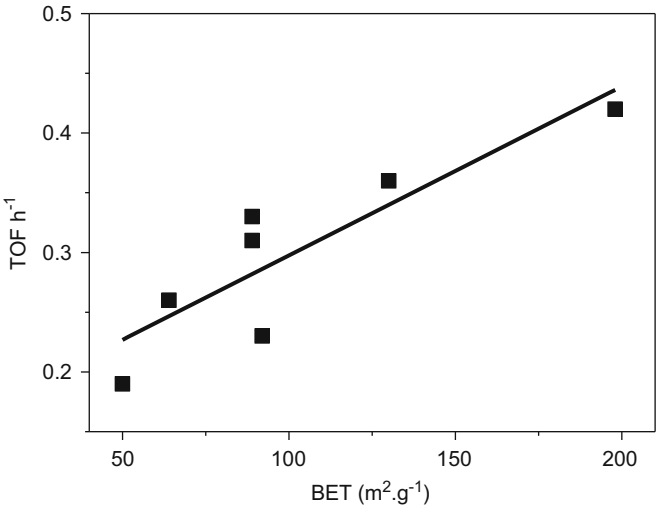

Fig. 9. Linear fit of the TOF factor and the BET surface areas.

areas, we found that the catalytic activity was inclined to be linearly dependent on the BET surface areas, as shown in Fig. 9. Thus, the BET surface areas mainly contributed to their catalytic activities.

4. Conclusions

The morphological and structural evolution of α-MnO_2 nanorods were tracked by XRD, SEM, TEM and BET. The crystallization of α-MnO_2 nanorods was found to proceed through three steps: an amorphous or poorly ordered nuclei formed first, then hollow nanospheres consisting of γ-MnO_2 nanorods formed second via a Ostwald ripening process, and the hollow nanospheres collapsed, the γ-MnO_2 nanorods finally transformed into the α-MnO_2 nanorods by a short-range rearrangement of MnO_6 octahedra. An increase in reaction temperature and reaction time promoted the phase transformation from γ-MnO_2 to α-MnO_2 nanorods. Increasing reaction temperature is more effective than increasing reaction time in the phase transformation. The catalytic activities of the MnO_2 structures prepared under different conditions in the aerobic oxidation of benzyl alcohol were mainly dependent on their BET surface areas.

References

[1] A.N. Goldsterm, Handbook of Nanophase Materials, Marcel Dekker, New York, 1997.
[2] H.G. Yang, C.H. Sun, S.Z. Qiao, J. Zou, G. Liu, S.C. Smith, H.M. Cheng, G.Q. Lu, Nature 453 (2008) 638.
[3] H.G. Yang, G. Liu, S.Z. Qiao, C.H. Sun, Y.G. Jin, S.C. Smith, J. Zou, H.M. Cheng, G.Q. Lu, J. Am. Chem. Soc. 131 (2009) 4078.
[4] E. Matijevic, P. Scheiner, J. Colloid Interface Sci. 63 (1978) 509.
[5] D. Portehault, S. Cassaignon, E. Baudrin, J.P. Jolivet, J. Mater. Chem. 19 (2009) 2407.
[6] X. Wang, Y.D. Li, Chem. Commun. 7 (2002) 764.
[7] D.B. Wang, C.X. Song, Z.S. Hu, X. Fu, J. Phys. Chem. B 109 (2005) 1125.
[8] L.N. Ye, C.Z. Wu, W. Guo, Y. Xie, Chem. Commun. 45 (2006) 4738.
[9] M.M. Thackeray, Prog. Solid State Chem. 25 (1997) 1.
[10] S. Sithambaram, R. Kumar, Y.C. Son, S.L. Suib, J. Catal. 253 (2008) 269.
[11] J.E. Post, Proc. Natl. Acad. Sci. USA. 96 (1999) 3447.
[12] F. Jiao, P.G. Bruce, Adv. Mater. 19 (2007) 657.
[13] T. Gao, H. Fjellvag, P. Norby, Nanotechnology 20 (2009) 7.
[14] Y.S. Ding, X.F. Shen, S. Gomez, H. Luo, M. Aindow, S.L. Suib, Adv. Funct. Mater. 16 (2006) 549.
[15] Y. Moritomo, A. Asamitsu, H. Kuwahara, Y. Tokura, Nature 380 (1996) 141.
[16] B. Ammundsen, J. Paulsen, Adv. Mater. 13 (2001) 943.
[17] X. Wang, Y.D. Li, Chem.- Eur. J. 9 (2003) 300.
[18] G.Q. Zhang, S.J. Bao, X.G. Zhang, H.L. Li, J. Solid State Electrochem. 9 (2005).
[19] L.C. Zhang, Z.H. Liu, H. Lv, X.H. Tang, K. Ooi, J. Phys. Chem. C 111 (2007) 8418.
[20] X.M. Liu, S.Y. Fu, C.J. Huang, Powder Technol. 154 (2005) 120.
[21] D. Portehault, S. Cassaignon, E. Baudrin, J.P. Jolivet, Chem. Mat. 20 (2008) 6140.
[22] D. Portehault, S. Cassaignon, N. Nassif, E. Baudrin, J.P. Jolivet, Angew. Chem.- Int. Edit. 47 (2008) 6441.
[23] D. Portehault, S. Cassaignon, E. Baudrin, J.P. Jolivet, Cryst. Growth Des. 9 (2009) 2562.
[24] X.B. Fu, J.Y. Feng, H. Wang, K.M. Ng, Catal. Commun. 10 (2009) 1844.
[25] X.B. Fu, J.Y. Feng, H. Wang, K.M. Ng, Nanotechnology 20 (2009) 9.
[26] J.C. Villegas, L.J. Garces, S. Gomez, J.P. Durand, S.L. Suib, Chem. Mat. 17 (2005) 1910.
[27] X.F. Shen, Y.S. Ding, J.C. Hanson, M. Aindow, S.L. Suib, J. Am. Chem. Soc. 128 (2006) 4570.
[28] Y.J. Xiong, Y. Xie, Z.Q. Li, C.Z. Wu, Chem.- Eur. J. 9 (2003) 1645.
[29] D. Portehault, S. Cassaignon, E. Baudrin, J.P. Jolivet, Chem. Mat. 19 (2007) 5410.
[30] P.M. De Wolff, Acta Crystallogr. 12 (1959) 341.
[31] Y.C. Son, V.D. Makwana, A.R. Howell, S.L. Suib, Angew. Chem.- Int. Edit. 40 (2001) 4280.